Stac3 has a direct role in skeletal muscle-type excitation–contraction coupling that is disrupted by a myopathy-causing mutation

Alexander Polster[a], Benjamin R. Nelson[b], Eric N. Olson[b], and Kurt G. Beam[a,1]

[a]Department of Physiology and Biophysics, University of Colorado Anschutz Medical Campus, Aurora, CO 80045; and [b]Department of Molecular Biology, University of Texas Southwestern Medical Center, Dallas, TX 75390

Contributed by Kurt G. Beam, August 2, 2016 (sent for review June 30, 2016; reviewed by Paul Brehm and Manfred Grabner)

In skeletal muscle, conformational coupling between $Ca_V1.1$ in the plasma membrane and type 1 ryanodine receptor (RyR1) in the sarcoplasmic reticulum (SR) is thought to underlie both excitation–contraction (EC) coupling Ca^{2+} release from the SR and retrograde coupling by which RyR1 increases the magnitude of the Ca^{2+} current via $Ca_V1.1$. Recent work has shown that EC coupling fails in muscle from mice and fish null for the protein Stac3 (SH3 and cysteine-rich domain 3) but did not establish the functional role of Stac3 in the $Ca_V1.1$–RyR1 interaction. We investigated this using both tsA201 cells and Stac3 KO myotubes. While confirming in tsA201 cells that Stac3 could support surface expression of $Ca_V1.1$ (coexpressed with its auxiliary β_{1a} and α_2-δ_1 subunits) and the generation of large Ca^{2+} currents, we found that without Stac3 the auxiliary γ_1 subunit also supported membrane expression of $Ca_V1.1/\beta_{1a}/\alpha_2$-$\delta_1$, but that this combination generated only tiny Ca^{2+} currents. In Stac3 KO myotubes, there was reduced, but still substantial $Ca_V1.1$ in the plasma membrane. However, the $Ca_V1.1$ remaining in Stac3 KO myotubes did not generate appreciable Ca^{2+} currents or EC coupling Ca^{2+} release. Expression of WT Stac3 in Stac3 KO myotubes fully restored Ca^{2+} currents and EC coupling Ca^{2+} release, whereas expression of $Stac3_{W280S}$ (containing the Native American myopathy mutation) partially restored Ca^{2+} currents but only marginally restored EC coupling. We conclude that membrane trafficking of $Ca_V1.1$ is facilitated by, but does not require, Stac3, and that Stac3 is directly involved in conformational coupling between $Ca_V1.1$ and RyR1.

L-type Ca^{2+} channels | Stac3 protein | excitation–contraction coupling

In skeletal muscle, the link between electrical excitation and contraction [excitation–contraction (EC) coupling] depends upon specialized junctions between the sarcoplasmic reticulum (SR) and the plasma membrane. It has been known for nearly 30 y that $Ca_V1.1$ (α_{1S}) functions in the plasma membrane as both a slowly activating L-type Ca^{2+} channel and as the trigger that activates Ca^{2+} release from the SR via the type 1 ryanodine receptor (RyR1), a process that is thought to involve conformational coupling between the two proteins (1). Thus, the KO of either protein results in the ablation of EC coupling (1, 2). Of the three $Ca_V1.1$ auxiliary subunits (α_2-δ_1, β_{1a}, and γ_1; for a review see ref. 3), only β_{1a} seems to be essential. Thus, KO of γ_1 (4, 5) or knockdown of α_2-δ_1 (6, 7) does not have major effects on the EC coupling and channel functions of $Ca_V1.1$, whereas KO of β_{1a} causes the loss of EC coupling (8). In part, this is because β_{1a} is required for efficient trafficking of $Ca_V1.1$ to the plasma membrane (9). However, β_{1a} also seems to play a more direct role because constructs lacking the appropriate β_{1a} sequence are able to restore membrane expression of $Ca_V1.1$ without restoring EC coupling (10, 11).

Work over the last few years has identified Stac3 (SH3 and cysteine-rich domain 3) as another protein of importance for EC coupling in skeletal muscle (12, 13). Stac3 belongs to a three-member family of proteins, contains a poly-glutamate domain, a PKC-C1–like domain, and two SH3 domains, and is expressed almost exclusively in skeletal muscle (12). Moreover, a point mutation (W284S) within the first SH3 domain is responsible for the severe, recessively inherited Native American myopathy (NAM) (13). Analysis of KO zebrafish and mice indicated that Stac3 is required for EC coupling but did not establish the mechanistic basis for this requirement. Subsequent experiments on heterologous expression in fibroblastic cells raised the possibility that Stac3 is important for membrane trafficking of $Ca_V1.1$ (14). Specifically, that work demonstrated that when $Ca_V1.1$ was expressed (together with β_{1a} and α_2-δ_1) in tsA201 cells it was retained in the endoplasmic reticulum unless Stac3 was also present.

Interestingly, the behavior of $Ca_V1.1$ in tsA201 cells showed some important differences from that of $Ca_V1.1$ in muscle cells. One difference is that the Ca^{2+} currents in tsA201 cells expressing $Ca_V1.1$, β_{1a}, α_2-δ_1, and Stac3 were slowly activating and of large amplitude (relative to gating charge movements) despite the absence of RyR1 in these cells, whereas in muscle cells the absence of RyR1 not only eliminates EC coupling but also causes the Ca^{2+} current via $Ca_V1.1$ to activate rapidly and to be of small amplitude (15, 16). Another issue arising from the comparison of results from tsA201 cells and muscle cells is whether membrane trafficking of $Ca_V1.1$ is strictly dependent on the presence of Stac3. In particular, Western blotting demonstrated that $Ca_V1.1$ is still present (at a reduced level) in E18.5, Stac3-KO tongue muscle (figure S8 in ref. 12). Accordingly, it may be that Stac3 is not the only factor in muscle cells that facilitates expression of $Ca_V1.1$.

In light of the previous work, a major goal of the present study was to resolve questions about the role of Stac3 in controlling membrane trafficking and function of $Ca_V1.1$ in both tsA201 cells and myotubes and to characterize the effects on $Ca_V1.1$ function of the NAM mutation of Stac3 (W280S in the mouse sequence). In both cell types, we used the magnitude of gating charge movements as an indicator of membrane expression of $Ca_V1.1$. Additionally, in the tsA201 cells we tested the inclusion of

Significance

Recent work showed that absence of the protein Stac3 (SH3 and cysteine-rich domain 3) caused a failure of excitation–contraction (EC) coupling in skeletal muscle but not whether this failure was because the trafficking of other key proteins was altered or because Stac3 plays a direct role in coupling $Ca_V1.1$ (the "sensor" of excitation) to RyR1 (type 1 ryanodine receptor, the Ca^{2+} release channel). Here we show that reduced expression of $Ca_V1.1$ could not account for the loss of EC coupling. Ca^{2+} release was fully restored by WT Stac3 but only marginally by Stac3 bearing a point mutation causing Native American myopathy. Thus, Stac3 seems to be involved directly in the coupling of $Ca_V1.1$ to RyR1.

Author contributions: A.P. and K.G.B. designed research; A.P. and K.G.B. performed research; B.R.N. and E.N.O. contributed new reagents/analytic tools; A.P. and K.G.B. analyzed data; and A.P. and K.G.B. wrote the paper.

Reviewers: P.B., Vollum Institute; and M.G., Innsbruck Medical University.

The authors declare no conflict of interest.

[1]To whom correspondence should be addressed. Email: Kurt.Beam@ucdenver.edu.

This article contains supporting information online at www.pnas.org/lookup/suppl/doi:10.1073/pnas.1612441113/-/DCSupplemental.

the γ_1 auxiliary subunit, which had been omitted in the previous work. We found that the presence of the γ_1 subunit (together with $Ca_V1.1$, β_{1a}, α_2-δ_1, and Stac3) caused Ca^{2+} currents via $Ca_V1.1$ to have rapid activation kinetics quantitatively similar to those of Ca^{2+} currents in myotubes lacking RyR1. The coexpression of γ_1 with $Ca_V1.1$, β_{1a}, and α_2-δ_1 without Stac3 resulted in substantial gating charge movements but only tiny Ca^{2+} ionic currents, consistent with the hypotheses that γ_1 is sufficient to support robust membrane expression of $Ca_V1.1$ and that the channel properties of $Ca_V1.1$ are interactively regulated by γ_1, Stac3, and RyR1. Consistent with the first hypothesis, gating charge movements were reduced by only about 50% in Stac3 KO myotubes (relative to Stac3 heterozygous myotubes). Strikingly, the $Ca_V1.1$ present in Stac3 KO myotubes seemed unable to mediate EC coupling and produced only small, rapidly activating Ca^{2+} currents. Expression of WT Stac3 in Stac3 KO myotubes fully restored both functions of $Ca_V1.1$, whereas expression of $Stac3_{W280S}$ caused a partial recovery of normal Ca^{2+} currents but very weak restoration of EC coupling. Taken together, our results indicate that Stac3 is required for both the normal Ca^{2+} channel and EC coupling functions of $Ca_V1.1$ and that these two effects of Stac3 rely on domains that are at least partially independent of one another.

Results

The γ_1 Auxiliary Subunit Regulates $Ca_V1.1$ Function and Membrane Trafficking in tsA201 Cells. Previously, we showed that Stac3 enabled robust, functional expression in tsA201 cells of $Ca_V1.1$ (with the β_{1a} and α_2-δ_1 auxiliary subunits also present), whereas functional expression did not occur in cells transfected only with $Ca_V1.1$, β_{1a}, and α_2-δ_1 (14). In fact, the L-type Ca^{2+} currents in cells transfected with $Ca_V1.1$, β_{1a}, α_2-δ_1, and Stac3 had amplitude (normalized by maximal gating charge) and kinetics indistinguishable from those of $Ca_V1.1$ exogenously expressed in dysgenic myotubes, which contain endogenous RyR1 (14). This result was surprising because tsA201 cells lack RyR1, and the absence of RyR1 in myotubes causes the L-type Ca^{2+} currents to activate much more rapidly and have substantially reduced amplitude (15, 16). Thus, we hypothesized that RyR1 somehow relieves the inhibitory effect of another protein that is present in myotubes and absent in tsA201 cells. An obvious candidate is the remaining $Ca_V1.1$ auxiliary subunit, γ_1, which we had omitted in the previous experiments because its KO was reported to have only modest effects on Ca^{2+} currents in mouse skeletal muscle (4, 5, 17).

Fig. 1 compares tsA201 cells transfected with YFP-$Ca_V1.1$, β_{1a}, α_2-δ_1, and Stac3 either without γ_1 (blue) or with γ_1 additionally present (orange). The additional presence of γ_1 caused a decrease in Ca^{2+} current amplitude (Fig. 1*A*), which seemed to be a consequence of reduced membrane expression of $Ca_V1.1$ inasmuch as there was a corresponding decrease in the magnitude of gating charge movement (Fig. 1*B*). Consequently, the ratio G_{max}/Q_{max}, which was determined by fitting Eqs. **1** and **2** to the peak I–V and peak Q–V relationships, respectively, was little affected by the additional presence of γ_1 and remained similar to that of $Ca_V1.1$ expressed in RyR1-containing, dysgenic myotubes (Fig. 2*A*, colors as in Fig. 1). However, the additional presence of γ_1 did cause a substantial acceleration of activation kinetics, which became very similar to those of Ca^{2+} currents produced by $Ca_V1.1$ endogenously expressed in RyR1-null (dyspedic) myotubes (Fig. 2 *B* and *C*). Thus, the addition of γ_1 recapitulated the faster activation resulting from the absence of RyR1 but not the reduced ratio of Ca^{2+} conductance to charge movement, suggesting that additional inhibitory elements may interact with $Ca_V1.1$ in native muscle cells.

For completeness, we also examined tsA201 cells transfected with YFP-$Ca_V1.1$, β_{1a}, α_2-δ_1, and γ1 without Stac3. We found that these cells produced very small, but still detectable, Ca^{2+} currents (Fig. 3*A*). The small size of these currents did not seem to be a consequence of low membrane expression because substantial charge movement was present in the cells transfected with YFP-$Ca_V1.1$, β_{1a}, α_2-δ_1, and γ1 (Fig. 3*B* and Table S1). Thus, γ1 seemed to be sufficient to support substantial membrane expression of CaV1.1 without Stac3, as was also evident from images of tsA201 cells transfected with fluorescently tagged constructs. These images revealed that the γ1–BFP (blue fluorescent protein) trafficked efficiently to the surface in the absence of other channel subunits (Fig. S1, *Left*) and that its presence together with the other auxiliary subunits caused YFP-$Ca_V1.1$ to traffic to the surface (Fig. S1, *Right*).

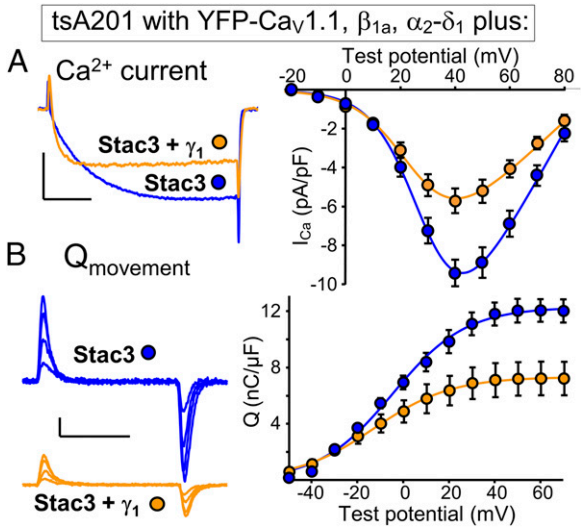

Fig. 1. The γ_1 subunit alters the kinetics of Ca^{2+} current via $Ca_V1.1$ in tsA201 cells. (*A*) Representative peak calcium currents (*Left*) and peak I-V relationships (*Right*) in tsA201 cells transfected with YFP-$Ca_V1.1$, β_{1a}, and α_2-δ_1 together with Stac3 alone, or with both Stac3 and γ_1. Test potentials: +40 mV; calibrations: 5 pA/pF (vertical), 50 ms (horizontal). (*B*) Representative charge movements (*Left*, V_{test} of −20, 0, +20, and +40 mV) and average Q-V relationships (*Right*) in tsA201 cells transfected with YFP-$Ca_V1.1$, β_{1a}, and α_2-δ_1 together with Stac3 alone, or with both Stac3 and γ_1. Calibrations: 2 pA/pF (vertical), 10 ms (horizontal).

Normal Functioning of $Ca_V1.1$ in Muscle Requires Stac3. Given the ability of exogenous γ1 to support membrane trafficking of $Ca_V1.1$ in tsA201 cells, we hypothesized that endogenous γ1 would cause $Ca_V1.1$ to be present in the plasma membrane of muscle cells null for Stac3. Thus, we compared myotubes obtained from mice homozygous for Stac3 KO with myotubes from their phenotypically normal, Stac3-heterozygous littermates (12). As we hypothesized, gating charge movement was present in Stac3 KO myotubes (Fig. 4*A*) Q_{max} = 3.7 ± 0.3 nC/μF, n = 8), albeit at a reduced level compared with that in Stac3 heterozygous myotubes Q_{max} = 7.9 ± 0.5 nC/μF, n = 9, Table S1). Therefore, Stac3 facilitates, but is not required for, $Ca_V1.1$ membrane expression. Despite substantial expression, however, $Ca_V1.1$ function was strongly altered in Stac3 KO myotubes. In particular, Ca^{2+} currents in Stac3 KO myotubes displayed a reduction in size that was larger than one would predict from the reduction in charge movement, as well as more rapid activation (Fig. 4*B*). More specifically, the Ca^{2+} currents in Stac3 KO myotubes were quantitatively similar to dyspedic (RyR1-null) myotubes with respect to both magnitude and activation kinetics (Fig. 2, black and white bars). Thus, Stac3 may be involved in the retrograde signal whereby RyR1 slows activation, and increases the amplitude, of L-type Ca^{2+} current via $Ca_V1.1$.

The central function of $Ca_V1.1$ is as the voltage sensor for EC coupling, which has been shown to fail in both zebrafish (13) and mice (12) null for Stac3. For example, the application of 120 mM K^+ produced only negligible Ca^{2+} transients in Stac3 KO myotubes (12). Here, we have measured Ca^{2+} transients in response to 200-ms

PHYSIOLOGY

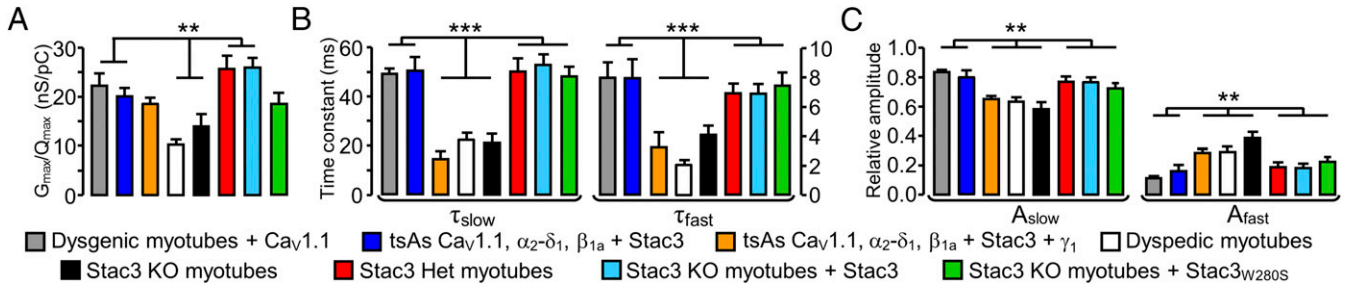

Fig. 2. (*A*) G_{max}/Q_{max} for the indicated combinations of cell type and construct. Values of G_{max} and Q_{max} (and thus G_{max}/Q_{max}) were obtained only from cells in which both peak I-V and Q-V relationships were measured. ** indicates a statistically significant difference ($P < 0.05$) between the center two combinations and the indicated combinations flanking them to the left and right. The G_{max}/Q_{max} ratios were not corrected for any background charge (unrelated to $Ca_V1.1$), which was small in dysgenic myotubes in the current experiments (0.83 ± 0.16 nC/μF, $n = 7$, measured at +40 mV). (*B* and *C*) Time constants and relative amplitudes, respectively, derived from a double-exponential function (Eq. **3**) fitted to Ca^{2+} currents at +40 mV. There was a statistically significant difference (***$P < 0.001$; **$P < 0.05$) between the center three combinations and the indicated combinations flanking them to the left and right. Numbers of cells (from left to right): 9 [dysgenic ($Ca_V1.1$-null) myotubes expressing YFP-$Ca_V1.1$], 10 (tsA201 cells expressing YFP-$Ca_V1.1$, α_2-δ_1, β_{1a} + Stac3), 9 (tsA201 cells expressing YFP-$Ca_V1.1$, α_2-δ_1, β_{1a} + Stac3 + γ_1), 7 [dyspedic (RyR1-null) myotubes], 7 (Stac3 KO myotubes), 9 (Stac3 heterozygous myotubes), 10 (Stac3 KO myotubes expressing WT Stac3), and 6 (Stac3 KO myotubes expressing $Stac3_{W280S}$).

depolarizing pulses to varying potentials, applied by means of whole-cell voltage clamping. We found that Stac3 heterozygous myotubes produced robust transients, which increased in size as a sigmoidal function of test potential, whereas no obvious response was observed in Stac3 KO myotubes (Fig. 4*C*). In principle, the failure of EC coupling Ca^{2+} release in the Stac3 KO myotubes could have been because $Ca_V1.1$ failed to localize at plasma membrane/SR junctions. To assess junctional targeting, we used a monoclonal antibody to $Ca_V1.1$ (18). Immunostaining with this antibody revealed that $Ca_V1.1$ was arrayed in discrete puncta in both Stac3 heterozygous and Stac3 KO myotubes (Fig. 5), which is consistent with junctional targeting (19). Thus, it seems that Stac3 is not required for junctional targeting but is essential for the EC coupling function of $Ca_V1.1$.

A Myopathy-Causing Mutation of Stac3 Profoundly Impairs EC Coupling. Horstick et al. (13) identified a missense mutation (W284S) of human Stac3 that causes a severe, recessively inherited myopathy, termed NAM (20). Additionally, they showed that EC coupling was diminished in fast-twitch muscle fibers expressing $Stac3^{NAM}$ compared with WT Stac3. The effects of the NAM mutation on L-type Ca^{2+} currents could not be addressed in their work because zebrafish $Ca_V1.1$ carries pore mutations that eliminate ionic current (21). Here, we introduced the NAM mutation

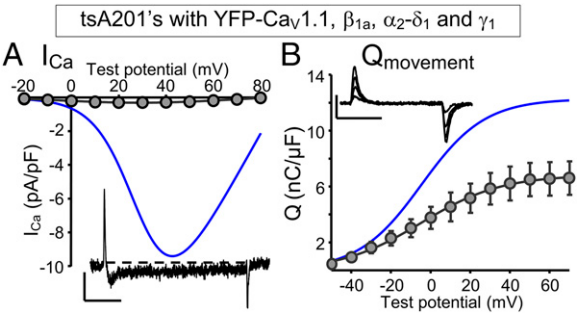

Fig. 3. The γ_1 subunit supports membrane expression of $Ca_V1.1$ in tsA201 cells. (*A*) Representative peak calcium current (test potential: +30 mV) and peak I-V relationships in tsA201 cells transfected with YFP-$Ca_V1.1$, β_{1a}, and α_2-δ_1 and γ_1. Calibrations: 1 pA/pF (vertical), 50 ms (horizontal). (*B*) Representative charge movements (V_{test} of −20, 0, +20, and +40 mV) and average Q-V relationships in tsA201 cells transfected with YFP-$Ca_V1.1$, β_{1a}, α_2-δ_1 and γ_1. Calibrations: 2 pA/pF (vertical), 10 ms (horizontal). For comparison, the smooth curves fitted to the peak I-V and Q-V data for tsA201 cells transfected with YFP-$Ca_V1.1$, β_{1a}, α_2-δ_1 and WT Stac3 (Fig. 1 *A* and *B*) are replotted in blue.

into the homologous position (W280S) of mouse Stac3 ($Stac3_{W280S}$) and characterized it both in tsA201 cells and in murine Stac3 KO myotubes. In tsA201 cells, $Stac3_{W280S}$ was less effective than WT Stac3 in supporting membrane expression of YFP-$Ca_V1.1$ (Fig. S2*A*), and L-type Ca^{2+} currents (Fig. S2*B*), such that Q_{max} and peak Ca^{2+} current were reduced by ∼65% and ∼75%, respectively, compared with WT Stac3 (Table S1). Additionally, activation of the L-type current was considerably more rapid for $Stac3_{W280S}$ than for WT Stac3 in tsA201 cells (gray and blue traces, respectively, Fig. S2*B*, *Left*). After expression in Stac3 KO myotubes, the differences between WT Stac3 and $Stac3_{W280S}$ with respect to charge movement and Ca^{2+} current were less pronounced than in the tsA201 cells. Specifically, in the Stac3 KO myotubes, Q_{max} was reduced only about 20% for $Stac3_{W280S}$ compared with WT Stac3 (Fig. 6*A* and Table S1), which is not entirely surprising because there was substantial charge movement present in the KO myotubes that completely lack Stac3. The NAM mutation also seemed to have less of an effect on the L-type Ca^{2+} current in myotubes than in tsA201 cells. In Stac3 KO myotubes, peak Ca^{2+} current was reduced about 50% for $Stac3_{W280S}$ (Fig. 6*B*). As a result the ratio of the L-type Ca^{2+} conductance to gating charge (G_{max}/Q_{max}) was reduced ∼30% compared with WT Stac3 and increased ∼35% compared with Stac3 KO myotubes (Fig. 2*A*). Although $Stac3_{W280S}$ caused only a partial recovery of Ca^{2+} current amplitude in Stac3 KO myotubes, it caused an almost complete restoration of slow activation kinetics. As described above, activation was rapid in Stac3 KO myotubes (Fig. 4*B*). These kinetics were slowed to a comparable extent by the expression of either $Stac3_{W280S}$ or WT Stac3 (Figs. 6*B* and 2 *B* and *C*). Although $Stac3_{W280S}$ caused a partial recovery of L-type Ca^{2+} in Stac3 KO myotubes, it produced very little restoration of EC coupling Ca^{2+} release. In particular, WT Stac3 restored Ca^{2+} transients in Stac3 KO myotubes that were almost as large as those in Stac3 heterozygous myotubes, whereas the Ca^{2+} transients in Stac3 KO myotubes expressing $Stac3_{W280S}$ were almost 10 times smaller (Fig. 6*C* and Table S2). The differential deficits in L-type Ca^{2+} current and EC coupling that result from the NAM mutation suggest that distinct domains of Stac3 regulate these two functions of $Ca_V1.1$.

Discussion

In this study we have used expression in tsA201 cells and Stac3-null myotubes to investigate the role of Stac3 in controlling the membrane trafficking and function of $Ca_V1.1$. In tsA201 cells, $Ca_V1.1$ did not traffic to the plasma membrane when coexpressed with only β_{1a} and α_2-δ_1 (14), but the additional presence of either Stac3 or the γ_1 auxiliary subunit was sufficient to support robust membrane expression of $Ca_V1.1$ (Figs. 1 and 3).

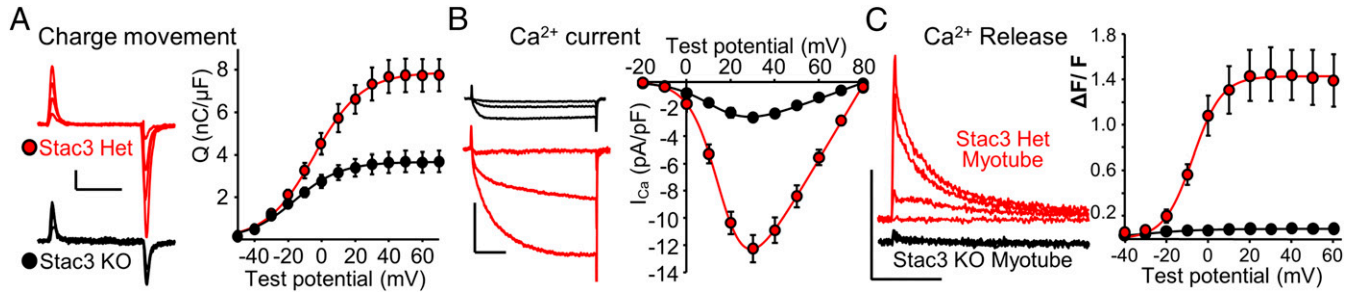

Fig. 4. The absence of Stac3 in myotubes partially reduces $Ca_V1.1$ membrane expression, significantly alters L-type Ca^{2+} current, and abolishes EC coupling Ca^{2+} release. (*A*) Representative charge movements (V_{test} of −20, 0, +20, and +40 mV, *Left*) and average Q-V relationships (*Right*) in myotubes homo- or heterozygous for a null mutation of Stac3. Calibrations: 1 pA/pF (vertical), 10 ms (horizontal). (*B*) Representative Ca^{2+} currents (V_{test} of −10, +10 and +30 mV, *Left*), and average peak I-V relationships (*Right*) in myotubes homo- or heterozygous for Stac3 KO. Calibrations: 5 pA/pF (vertical), 50 ms (horizontal). (*C*) Representative whole-cell, voltage-clamp measurements of Ca^{2+} transients with Fluo-3 (200 ms depolarizations from −80 mV to −40, −20, 0, and +20 mV, *Left*) and average peak change in fluorescence normalized by baseline ($\Delta F/F$) as a function of test potential (*Right*) for heterozygous or homozygous Stac3 KO myotubes. Calibrations: 1 $\Delta F/F$ (vertical), 5 s (horizontal).

However, the L-type Ca^{2+} current differed dramatically for the two situations, being large and slowly activating with Stac3 (Fig. 1*A*) and extremely small with γ_1 (Fig. 3*A*). With both Stac3 and γ_1 present, the L-type current was large but activated rapidly (Fig. 1*A*). Thus, Stac3 and γ_1 interactively regulate the expression and channel function of $Ca_V1.1$ in tsA201 cells.

In Stac3 KO myotubes, $Ca_V1.1$ was still present in the plasma membrane, although at a somewhat reduced level (Fig. 4*A*). Based on the results from the tsA201 cells, it seems likely that this membrane expression of $Ca_V1.1$ in the KO myotubes was supported, at least in part, by endogenous γ_1. Significantly, the KO of Stac3 in myotubes caused a near-complete loss of EC coupling Ca^{2+} release despite the fact that the substantial amount of remaining $Ca_V1.1$ (Fig. 4*A*) seemed to be localized at plasma membrane junctions with the SR (Fig. 5). The functional consequences of the myopathy-causing NAM mutation provide further evidence that Stac3 plays an essential role in EC coupling. Although the expression of $Stac3_{W280S}$, which bears this mutation, resulted in reduced $Ca_V1.1$ gating charge movement in both tsA201 cells (Fig. S2) and Stac3 KO myotubes (Fig. 6), the reduction of EC coupling Ca^{2+} release in myotubes (87%, Table S2) was far greater than would have been expected from the reduction in charge movement (23%, Table S1), compared with those produced by expression of WT Stac3. In addition to being essential for orthograde (EC) coupling between $Ca_V1.1$ and RyR1, Stac3 also seemed to be important for the retrograde effect of RyR1 on the channel function of $Ca_V1.1$. In particular, the L-type Ca^{2+} current in Stac3 KO myotubes was small and rapidly activating (Fig. 4*B*), with an overall, quantitative similarity to the L-type current in dyspedic myotubes (Fig. 2, black and white bars, respectively). Thus, retrograde coupling seems to be abolished by the absence of Stac3.

In WT muscle cells, the conformational coupling of $Ca_V1.1$ to RyR1, which is thought to underlie EC coupling, had been shown to require the additional presence of the β_{1a} subunit (8, 9, 22). Our current results now indicate that Stac3 represents another necessary component of the molecular assembly that is conformationally coupled to RyR1. At this point, it is only possible to speculate about why Stac3 must be part of this complex. One possibility is that in the absence of Stac3, $Ca_V1.1$ and β_{1a} do not assume the conformations necessary for their coupling to RyR1. Another possibility is that Stac3 is interposed between $Ca_V1.1/\beta_{1a}$ and RyR1. Consistent with this possibility, Stac3 seems to bind to $Ca_V1.1$ both in RyR1 null ("dyspedic") myotubes and in tsA201 cells (14). However, Stac3 does not seem to bind to RyR1 either in $Ca_V1.1$-null ("dysgenic") myotubes or in tsA201 cells (14). Nonetheless, it remains possible that Stac3 could function as an intermediary between $Ca_V1.1/\beta_{1a}$ and RyR1 if one postulated that Stac3 can bind to RyR1 only when complexed with $Ca_V1.1/\beta_{1a}$.

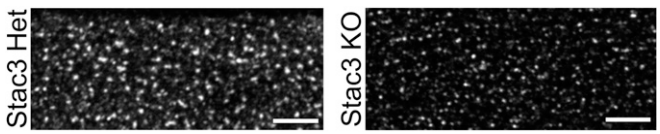

Fig. 5. $Ca_V1.1$ immunostaining in myotubes heterozygous (*Left*) or homozygous (*Right*) for Stac3 KO. (Scale bars: 5 μm.)

In dyspedic myotubes, which lack RyR1, the L-type Ca^{2+} current has more rapid activation kinetics and a reduced amplitude (G_{max}/Q_{max}, which is an indirect indicator of channel open probability). As a possible explanation, we have suggested that the presence of RyR1 relieves the inhibitory effect that one or more other junctional proteins have on $Ca_V1.1$ (14). In the present work, we considered whether the γ_1 auxiliary subunit of $Ca_V1.1$ might function in this way. Previously, the functional effects of the γ_1 subunit on $Ca_V1.1$ function had been investigated by analyzing myotubes or muscle fibers in which γ_1 had been knocked out. The KO of γ_1 caused the Ca^{2+} current via $Ca_V1.1$ in myotubes to be about one-third larger and to decay more slowly during prolonged pulses (4, 23). Additionally, the voltage for half-inactivation of current was positively shifted by ∼9 mV in γ_1 KO myotubes and ∼14 mV in γ_1 KO muscle fibers. Thus, these studies indicate that γ_1 promotes the inactivation of L-type Ca^{2+} current via $Ca_V1.1$ in muscle cells but leaves open the question of whether this inhibitory effect would, in the absence of RyR1, cause both reduced amplitude and faster activation of the L-type current via $Ca_V1.1$. The experiments on tsA201 cells indicate that this is not the case. Specifically, the transfection of γ_1 together with $Ca_V1.1$, β_{1a}, α_2-δ_1, and Stac3 resulted in currents that activated rapidly, like those in dyspedic myotubes (Figs. 1*A* and 2 *B* and *C*), but with a normalized amplitude (G_{max}/Q_{max}) little different from when γ_1 was not present (Fig. 2*A*, orange and blue) and similar to that of dysgenic myotubes expressing exogenous $Ca_V1.1$ (Fig. 2*A*, gray). A possible explanation for this result is that the kinetic effect of RyR1 involves γ_1 and that the G_{max}/Q_{max} effect involves another structural element within plasma membrane/SR junctions of muscle cells. This suggestion is consistent with the results of previous work analyzing the functional consequences of a mutation (E4242G) within RyR1. The conclusion from that work was that the retrograde effects of RyR1 on kinetics and amplitude are dependent on distinct structural elements within RyR1 (24). Independent of mechanistic interpretation, however, our results indicate, not surprisingly, that the environment of the $Ca_V1.1/\beta_{1a}/\alpha_2$-$\delta_1/\gamma_1$/Stac3 complex in tsA201 cells differs from that in myotubes. For instance, in tsA201 cells, the slowly

PHYSIOLOGY

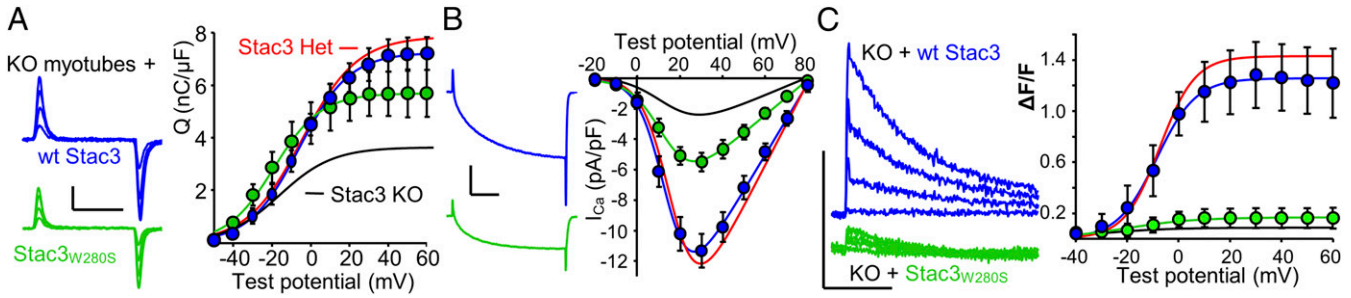

Fig. 6. In myotubes, the NAM mutation of Stac3 has modest effects on membrane expression of $Ca_V1.1$ and L-type current properties but causes a very large reduction in EC coupling Ca^{2+} release. (*A*) Representative charge movements (V_{test} of −20, 0, +20, and +40 mV, *Left*) and average Q-V relationships (*Right*) in Stac3 KO myotubes expressing WT Stac3 or $Stac3_{W280S}$. Calibrations: 2 pA/pF (vertical), 10 ms (horizontal). (*B*) Representative ionic peak currents at +30 mV (*Left*), and average peak I-V relationships (*Right*) for Stac3 KO myotubes expressing WT Stac3 or $Stac3_{W280S}$. Calibrations: 5 pA/pF (vertical), 50 ms (horizontal). (*C*) Representative whole-cell, voltage-clamp measurements of Ca^{2+} transients with Fluo-3 (200-ms depolarizations from −80 mV to −40, −20, 0, and +20 mV, *Left*) and average peak change in fluorescence normalized by baseline ($\Delta F/F$) as a function of test potential (*Right*) for Stac3 KO myotubes expressing WT Stac3 or $Stac3_{W280S}$. Calibrations: 1 $\Delta F/F$ (vertical), 5 s (horizontal). The smooth curves for data from myotubes heterozygous (red) and homozygous (black) for Stac3 KO are replotted from Fig. 4 *A*–*C*.

activating L-type current observed when $Ca_V1.1$, and β_{1a}, and α_2-δ_1 were coexpressed with WT Stac3 became rapidly activating upon substitution of the NAM mutant, $Stac3_{W280S}$ (Fig. S2*B*). By contrast, when $Stac3_{W280S}$ was expressed in Stac3 KO myotubes, the L-type current displayed slow activation kinetics that were nearly identical to those when WT Stac3 was expressed in the KO myotubes (Figs. 6*B* and 2 *B* and *C*). These differences may indicate that the relative stoichiometry of the transfected proteins in tsA201 cells differs from that of the same proteins endogenously expressed in muscle cells and/or that the interactions of these proteins are modified by additional proteins present in muscle cells.

An important goal for future research will be to identify the domains of Stac3 that govern its roles in EC coupling and in modulating the L-type Ca^{2+} current. Based on the differential effects of the NAM mutation on these two functions (Fig. 6 *B* and *C*), it seems possible that they depend on different regions of Stac3, but this will need to be tested more thoroughly. Because Stac3 seems to bind directly to $Ca_V1.1$ (14), an obvious next step will be to identify the regions of both proteins that underlie their binding to one another. This in turn will make it possible to determine whether domains of Stac3 found to be important for its binding to $Ca_V1.1$ correspond to the domains found to be important for its functional roles.

Materials and Methods

Molecular Biology. The construction of the expression plasmids for YFP-$Ca_V1.1$, unlabeled β_{1a}, and unlabeled Stac3 was described previously (14, 25, 26). To create Stac3-BFP, the Stac3 fragment from Stac3-YFP (14) was inserted into pmTagBFP2-N1 (Addgene) using the restriction enzymes NdeI + BamHI. For the γ_1 constructs, standard PCR was used to introduce KpnI sites, or KpnI sites and a stop codon, flanking the coding sequence for γ_1 (gene ID 100346309; Cedarlane Laboratories) from which the KpnI-KpnI fragment was inserted into TagBFP2-N1 to create γ_1-BFP or into pEYFP-N1 (Clontech). Afterward, the latter construct was digested with NdeI and BamHI, and the fragment containing the γ_1 sequence was then ligated to the 3,575-bp fragment of pEYFP-C1 (Clontech) that had been digested with the same enzymes to produce the expression vector for unlabeled γ_1. Unlabeled $Stac3_{W280S}$ and $Stac3_{W280S}$-BFP were created by using the QuikChange II site-directed mutagenesis kit (Agilent Technologies). The α_2-δ_1 subunit was kindly provided by William A. Sather, University of Colorado, Denver.

Primary Skeletal Muscle Cell Culture and cDNA Microinjection. Myoblasts from newborn dysgenic mice, homozygous for absence of $Ca_V1.1$ (1), newborn dyspedic mice, homozygous for absence of RyR1 (2, 27), or embryonic day-18.5 fetuses, homozygous or heterozygous for absence of Stac3, were prepared as described before (12, 28). Cultures were grown in high-glucose DMEM (Mediatech) supplemented with 10% (vol/vol) FBS and 10% (vol/vol) horse serum (both from HyClone Laboratories). After 4–5 d, this medium was replaced with differentiation medium [DMEM supplemented with 2% (vol/vol) horse serum]. Two to four days following the shift to differentiation medium, single nuclei were microinjected with plasmid cDNA (200 ng/μL in water). Forty-eight hours after injection, expressing cells were identified on the basis of YFP fluorescence.

tsA201 Cell Culture and Expression of cDNA. tsA201 cells were propagated in high-glucose DMEM supplemented with 10% (vol/vol) FBS and 2 mM glutamine. Cells were transfected by Lipofectamine 2000 (Life Technologies) with various combinations of YFP-$Ca_V1.1$ (1 μg per dish), β_{1a}, α_2-δ_1, Stac3, $Stac3_{W280S}$, γ_1, and γ_1-BFP (0.5 μg per dish) cDNA. Six hours following transfection, cells were removed from the dish, using Trypsin EDTA (Mediatech), and replated at ∼1×10^4 cells per 35-mm dish to obtain isolated cells for electrophysiological recording. Forty-eight hours following transfection, positively transfected cells were identified by the pattern of yellow fluorescence and were used for electrophysiology or imaging.

Immunostaining. Myotubes were washed twice with PBS containing (in millimolar) 137 NaCl, 2.7 KCl, 4.3 Na_2HPO_4, and 1.47 KH_2PO_4, pH to 7.4 with HCl, and fixed in paraformaldehyde [4% (vol/vol) in PBS]. After fixation, the cells were washed three times with PBS and incubated in 10% (vol/vol) goat serum/1% BSA/PBS for 60 min at room temperature. Incubation in mouse $Ca_V1.1$ subunit primary antibody IIF7 (1:500 diluted in 1% BSA/PBS), kindly provided by Kevin P. Campbell, University of Iowa, Iowa City, IA, was overnight at 4 °C, after which the cells were washed three times for 10 min with 1% BSA/PBS. Cells were then incubated in Alexa Fluor 568-labeled secondary antibody (Molecular Probes, diluted 1:300 in 1% BSA/PBS) for 1 h at room temperature, washed with 1% BSA/PBS (3 × 10 min, with gentle agitation), and imaged.

Confocal Microscopy. Myotubes or tsA201 cells were superfused with rodent Ringer's solution (146 mM NaCl, 5 mM KCl, 2 mM $CaCl_2$, 1 mM $MgCl_2$, and 10 mM Hepes, pH 7.4, with NaOH) and examined using a Zeiss LSM 710 confocal microscope. Images were obtained as a single optical slice with a 40× (1.3 N.A.) or 63× (1.4 N.A.) oil-immersion objective. Excitation and emission, respectively, were 405 nm (diode laser) and 415–448 nm for BFP, 514 nm (argon laser) and 530–565 nm for YFP, and 543 nm (HeNe laser) and 596–664 nm for Alexa Fluor 568.

Measurement of L-Type Ca^{2+} Currents and Intramembrane Charge Movements. All experiments were performed at room temperature (∼25 °C). Pipettes (∼2.0 MΩ) were filled with internal solution, which consisted of (in millimolar) 140 Cs-aspartate, 10 Cs_2-EGTA, 5 $MgCl_2$, and 10 Hepes, pH 7.4 with CsOH. The external solution contained (in millimolar) 145 tetraethylammonium-Cl, 10 $CaCl_2$, and 10 Hepes, pH 7.4 with tetraethylammonium-OH. For electrophysiological experiments on myotubes, 0.003 mM tetrodotoxin and 0.1 mM *N*-benzyl-*p*-toluene sulphonamide were added to the external solution. For the measurement of intramembrane charge movements attributable to $Ca_V1.1$, 0.1 mM $LaCl_3$ and 0.5 mM $CdCl_2$ were added to the bath solution, and voltage was stepped from the holding potential (−80 mV) to −20 mV for 1 s, repolarized to −50 mV for 50–80 ms, and then to varying depolarized test potentials (29). This same pulse protocol was used for the measurement of L-type Ca^{2+} currents in myotubes

to inactivate Na^+ channels and T-type Ca^{2+} channels; in tsA201 cells, L-type currents were measured in response to test pulses applied directly from the holding potential. Electronic compensation was used to reduce the effective series resistance to <5 MΩ (time constant <400 μs). Linear components of leak and capacitive current were corrected with −P/4 online subtraction protocols. Filtering was at 2–5 kHz and digitization was either at 10 kHz (L-type currents) or 25 kHz (charge movements). Cell capacitance was determined by integration of a transient elicited by stepping from the holding potential (−80 mV) to −70 mV using Clampex 8.2 (Molecular Devices) and was used to normalize charge movements (nanocoulombs per microfarad) and ionic currents (picoamperes per picofarad). Peak current-voltage (I-V) curves were fitted according to

$$I = G_{max}(V - V_{rev})/\{1 + \exp[-(V - V_{1/2})/k_G]\}, \quad [1]$$

where I is the peak current for the test potential V, V_{rev} is the reversal potential, G_{max} is the maximum Ca^{2+} channel conductance, $V_{1/2}$ is the half-maximal activation potential, and k_G is the slope factor. Plots of the integral of the ON transient (Q_{on}) of intramembrane charge movement as a function of test potential (V) were fitted according to

$$Q_{on} = Q_{max}/\{1 + \exp[(V_Q - V)/k_Q]\}, \quad [2]$$

where Q_{max} is the maximal Q_{on}, V_Q is the potential causing movement of half the maximal charge, and k_Q is a slope parameter. The activation phase of macroscopic ionic currents was fitted as described in ref. 16 using the following exponential function:

$$I(t) = A_{fast}[\exp(-t/\tau_{fast})] + A_{slow}[\exp(-t/\tau_{slow})] + C, \quad [3]$$

where $I(t)$ is the current at time t after the depolarization, A_{fast}, and A_{slow} are the steady-state current amplitudes of each component with their respective time constants of activation (τ_{fast} and τ_{slow}), and C represents the peak current.

Measurement of Intracellular Ca^{2+} Transients. Changes in intracellular Ca^{2+} were recorded with Fluo-3 (Molecular Probes) in the whole-cell patch-clamp configuration (discussed above). The salt form of the dye was added to the standard internal solution for a final concentration of 200 nM. After entry into the whole-cell configuration, a waiting period of >5 min was used to allow the dye to diffuse into the cell interior. A Zeiss LSM 710 was used to excite the dye (488 nm) and to measure fluorescence emission (519–585 nm) in the voltage-clamped myotube during 200-ms test pulses. Fluorescence data are expressed as $\Delta F/F$, where ΔF represents the change in peak fluorescence from baseline during the test pulse and F is the fluorescence immediately before the test pulse minus the average background (non–Fluo-3) fluorescence. The peak value of the fluorescence change ($\Delta F/F$) for each test potential (V) was fitted according to

$$(\Delta F/F) = (\Delta F/F)_{max}/\{1 + \exp[(V_F - V)/k_F]\}, \quad [4]$$

where $(\Delta F/F)_{max}$ is the maximal fluorescence change, V_F is the potential causing half the maximal change in fluorescence, and k_F is a slope parameter.

Analysis. The software program SigmaPlot (version 11.0; SSPS) was used for statistical analysis, curve fitting, and preparation of figures. All data are presented as mean ± SEM. Statistical comparisons were made by one-way ANOVA.

ACKNOWLEDGMENTS. We thank O. Moua for expert technical assistance. This work was supported by NIH Grants AR055104 and AR052354 and Muscular Dystrophy Association Grant MDA176448 (to K.G.B.). Work in the laboratory of E.N.O. was supported by NIH Grants HL-077439, HL-111665, HL-093039, DK-099653, and U01-HL-100401 and Robert A. Welch Foundation Grant 1-0025. B.R.N. was supported by an NIH predoctoral fellowship.

1. Tanabe T, Beam KG, Powell JA, Numa S (1988) Restoration of excitation-contraction coupling and slow calcium current in dysgenic muscle by dihydropyridine receptor complementary DNA. *Nature* 336(6195):134–139.
2. Takeshima H, et al. (1994) Excitation-contraction uncoupling and muscular degeneration in mice lacking functional skeletal muscle ryanodine-receptor gene. *Nature* 369(6481):556–559.
3. Arikkath J, Campbell KP (2003) Auxiliary subunits: Essential components of the voltage-gated calcium channel complex. *Curr Opin Neurobiol* 13(3):298–307.
4. Freise D, et al. (2000) Absence of the γ subunit of the skeletal muscle dihydropyridine receptor increases L-type Ca^{2+} currents and alters channel inactivation properties. *J Biol Chem* 275(19):14476–14481.
5. Ursu D, et al. (2001) Excitation-contraction coupling in skeletal muscle of a mouse lacking the dihydropyridine receptor subunit γ1. *J Physiol* 533(Pt 2):367–377.
6. Obermair GJ, et al. (2005) The Ca^{2+} channel $\alpha_2\delta$-1 subunit determines Ca^{2+} current kinetics in skeletal muscle but not targeting of α_{1S} or excitation-contraction coupling. *J Biol Chem* 280(3):2229–2237.
7. Gach MP, et al. (2008) $\alpha_2\delta_1$ dihydropyridine receptor subunit is a critical element for excitation-coupled calcium entry but not for formation of tetrads in skeletal myotubes. *Biophys J* 94(8):3023–3034.
8. Gregg RG, et al. (1996) Absence of the β subunit (cchb1) of the skeletal muscle dihydropyridine receptor alters expression of the α_1 subunit and eliminates excitation-contraction coupling. *Proc Natl Acad Sci USA* 93(24):13961–13966.
9. Strube C, Beurg M, Powers PA, Gregg RG, Coronado R (1996) Reduced Ca^{2+} current, charge movement, and absence of Ca^{2+} transients in skeletal muscle deficient in dihydropyridine receptor β_1 subunit. *Biophys J* 71(5):2531–2543.
10. Sheridan DC, Cheng W, Carbonneau L, Ahern CA, Coronado R (2004) Involvement of a heptad repeat in the carboxyl terminus of the dihydropyridine receptor β_{1a} subunit in the mechanism of excitation-contraction coupling in skeletal muscle. *Biophys J* 87(2):929–942.
11. Schredelseker J, Dayal A, Schwerte T, Franzini-Armstrong C, Grabner M (2009) Proper restoration of excitation-contraction coupling in the dihydropyridine receptor β_1-null zebrafish relaxed is an exclusive function of the β_{1a} subunit. *J Biol Chem* 284(2):1242–1251.
12. Nelson BR, et al. (2013) Skeletal muscle-specific T-tubule protein STAC3 mediates voltage-induced Ca^{2+} release and contractility. *Proc Natl Acad Sci USA* 110(29):11881–11886.
13. Horstick EJ, et al. (2013) Stac3 is a component of the excitation-contraction coupling machinery and mutated in Native American myopathy. *Nat Commun* 4:1952.
14. Polster A, Perni S, Bichraoui H, Beam KG (2015) Stac adaptor proteins regulate trafficking and function of muscle and neuronal L-type Ca^{2+} channels. *Proc Natl Acad Sci USA* 112(2):602–606.
15. Nakai J, et al. (1996) Enhanced dihydropyridine receptor channel activity in the presence of ryanodine receptor. *Nature* 380(6569):72–75.
16. Avila G, Dirksen RT (2000) Functional impact of the ryanodine receptor on the skeletal muscle L-type $Ca(^{2+})$ channel. *J Gen Physiol* 115(4):467–480.
17. Held B, Freise D, Freichel M, Hoth M, Flockerzi V (2002) Skeletal muscle L-type $Ca(^{2+})$ current modulation in γ1-deficient and wildtype murine myotubes by the γ1 subunit and cAMP. *J Physiol* 539(Pt 2):459–468.
18. Leung AT, Imagawa T, Campbell KP (1987) Structural characterization of the 1,4-dihydropyridine receptor of the voltage-dependent Ca^{2+} channel from rabbit skeletal muscle. Evidence for two distinct high molecular weight subunits. *J Biol Chem* 262(17):7943–7946.
19. Flucher BE, Andrews SB, Daniels MP (1994) Molecular organization of transverse tubule/sarcoplasmic reticulum junctions during development of excitation-contraction coupling in skeletal muscle. *Mol Biol Cell* 5(10):1105–1118.
20. Stamm DS, et al. (2008) Native American myopathy: Congenital myopathy with cleft palate, skeletal anomalies, and susceptibility to malignant hyperthermia. *Am J Med Genet A* 146A(14):1832–1841.
21. Schredelseker J, Shrivastav M, Dayal A, Grabner M (2010) Non-Ca^{2+}-conducting Ca^{2+} channels in fish skeletal muscle excitation-contraction coupling. *Proc Natl Acad Sci USA* 107(12):5658–5663.
22. Beurg M, et al. (1999) Differential regulation of skeletal muscle L-type Ca^{2+} current and excitation-contraction coupling by the dihydropyridine receptor β subunit. *Biophys J* 76(4):1744–1756.
23. Ahern CA, et al. (2001) Modulation of L-type Ca^{2+} current but not activation of Ca^{2+} release by the gamma1 subunit of the dihydropyridine receptor of skeletal muscle. *BMC Physiol* 1:8.
24. Bannister RA, Sheridan DC, Beam KG (2016) Distinct components of retrograde $Ca_{(V)}$1.1-RyR1 coupling revealed by a lethal mutation in RyR1. *Biophys J* 110(4):912–921.
25. Papadopoulos S, Leuranguer V, Bannister RA, Beam KG (2004) Mapping sites of potential proximity between the dihydropyridine receptor and RyR1 in muscle using a cyan fluorescent protein-yellow fluorescent protein tandem as a fluorescence resonance energy transfer probe. *J Biol Chem* 279(42):44046–44056.
26. Leuranguer V, Papadopoulos S, Beam KG (2006) Organization of calcium channel β_{1a} subunits in triad junctions in skeletal muscle. *J Biol Chem* 281(6):3521–3527.
27. Buck ED, Nguyen HT, Pessah IN, Allen PD (1997) Dyspedic mouse skeletal muscle expresses major elements of the triadic junction but lacks detectable ryanodine receptor protein and function. *J Biol Chem* 272(11):7360–7367.
28. Beam KG, Franzini-Armstrong C (1997) Functional and structural approaches to the study of excitation-contraction coupling. *Methods Cell Biol* 52:283–306.
29. Adams BA, Tanabe T, Mikami A, Numa S, Beam KG (1990) Intramembrane charge movement restored in dysgenic skeletal muscle by injection of dihydropyridine receptor cDNAs. *Nature* 346(6284):569–572.